Polysaccharide - Modified MMT/ Modified MMT/ Polysaccharide – MNP, Lignin - Modified MMT Nanocomposites Verses Polyethyleneimineimine- Modified MMT-: A Comparative Analysis of Sustained Pesticide Delivery

Ritu Mahajan

Institute of Nano Science and Technology, Knowledge City, Sector 81, SAS Nagar, Manauli PO, Mohali, Punjab 140306, India

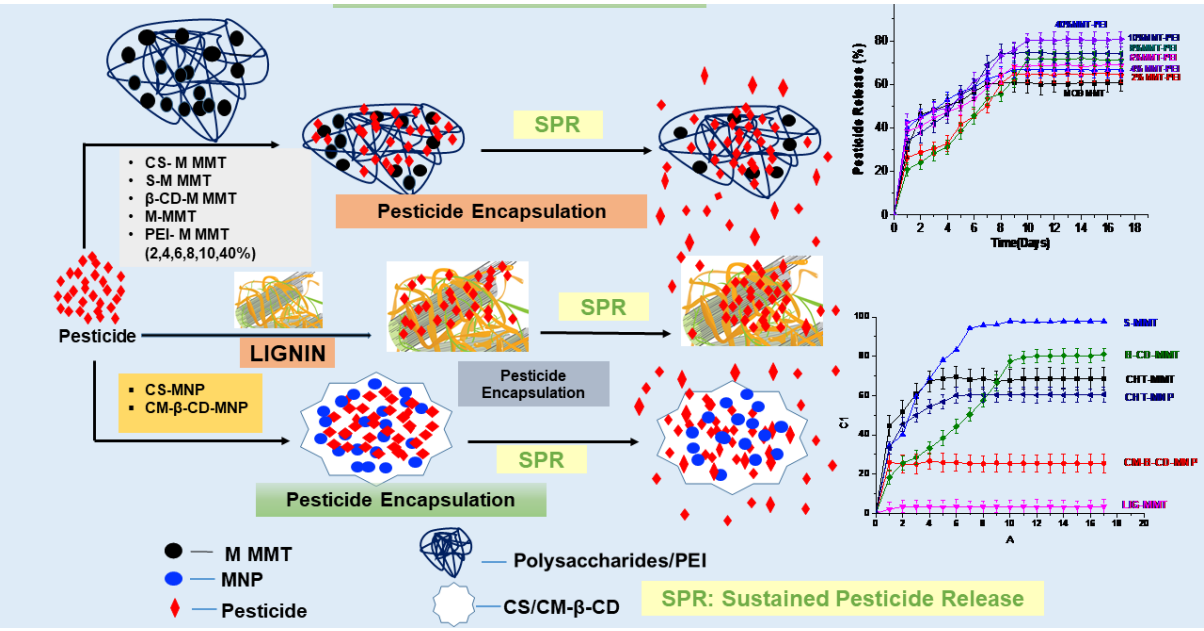

ABSTRACT: The substance properties can change drastically at the nanoscale. Materials can demonstrate new properties with just a reduction in size and no alteration in the substance itself. In this paper, modified montmorillonite (M MMT) and a variety of different hybrid natural-based nanocomposites were systematically investigated by combining a suspension of (M MMT) as a nanofiller with polymers comprising either chitosan (CS), starch (S), β-cyclodextrin (β-CD), polyethyleneimine (PEI), while in other cases polysaccharides such as chitosan (CS), carboxymethyl-β-cyclodextrin (CM-β-CD) served as the macroscopic polymer matrix while magnetite (MNP) constituted the nanoparticles thereby resulting in the polysaccharide-MNP nanocomposite. In the third case, the macroscopic polymer matrix of lignin mixed with M MMT suspension as nanofiller was analysed as controlled release formulations and the efficiencies of PLE and SPR for chlorpyrifos (ChP) pesticides were compared with gas chromatography mass spectrometry (GC-MS) and corrected with inductively coupled plasma mass spectrometry (ICP MS). Overall, owing to the smaller sized particles collected under optimum conditions, all inorganic and hybrid composites displayed decent to excellent PLE.

However, L-M MMT displayed an impressive median PLE of 98 % relative to other Polysaccharide-M MMTs (50-80 %), polysaccharide-MNPs (72-75 %), PEI-M MMT (61-76 %) among the hybrid composites tested together with M MMT (49 %). However, compared to other composites with SPR results of ChP of 98 % in 12 days, S-M MMT displayed comparatively better results while other synthesized inorganic and nanocomposites showed 26-81 % release. We expect that this description will help researchers choose the right approach for designing pesticides and achieving better pesticide delivery.

KEYWORDS: Chlorpyrifos, Polysaccharides, lignin, Magnetite, Polyethyleneimine, Modified Montmorillonite,

1. INTRODUCTION

Nanotechnology has risen to prominence in the last decade as a potential game-changer in agricultural practices.[1-3] Nanoscale particles have revolutionary properties that can increase pesticide efficiency and make the delivery system smart in terms of pesticide distribution. [4-5] Pesticides, like nano-drugs, can be administered in a regulated and targeted manner using a smart delivery system.[6-7]

Nanoclays, such as montmorillonite (MMT), serve as nanofillers in polymer matrixes such as polysaccharides.[8-9] Clay gallery swelling is induced by MMT alteration, which improves polysaccharide chain intercalation and clay dispersion in the polysaccharide gallery. Via modification and compounding with a polysaccharide, the silicate layers of MMT can be delaminated, resulting in a nanocomposite with improved tensile properties. [10-12] When MNP is used instead of MMT as a nanofiller, the polysaccharide coating on MNP not only offers stability, but also reduces the toxicity of bare MNP, allowing the formulation to reach the target directly.[13]

The incorporation of nanofillers such as M MMT into the PEI results in a substantial improvement in the elasticity module, increased thermal resilience or greater fire retardancy

factor. [14-16] PEIs and macroscopic polymer such as, lignin greatly improve a range of physicochemical properties needed in new fields of application. (Figure 1). [17-19]

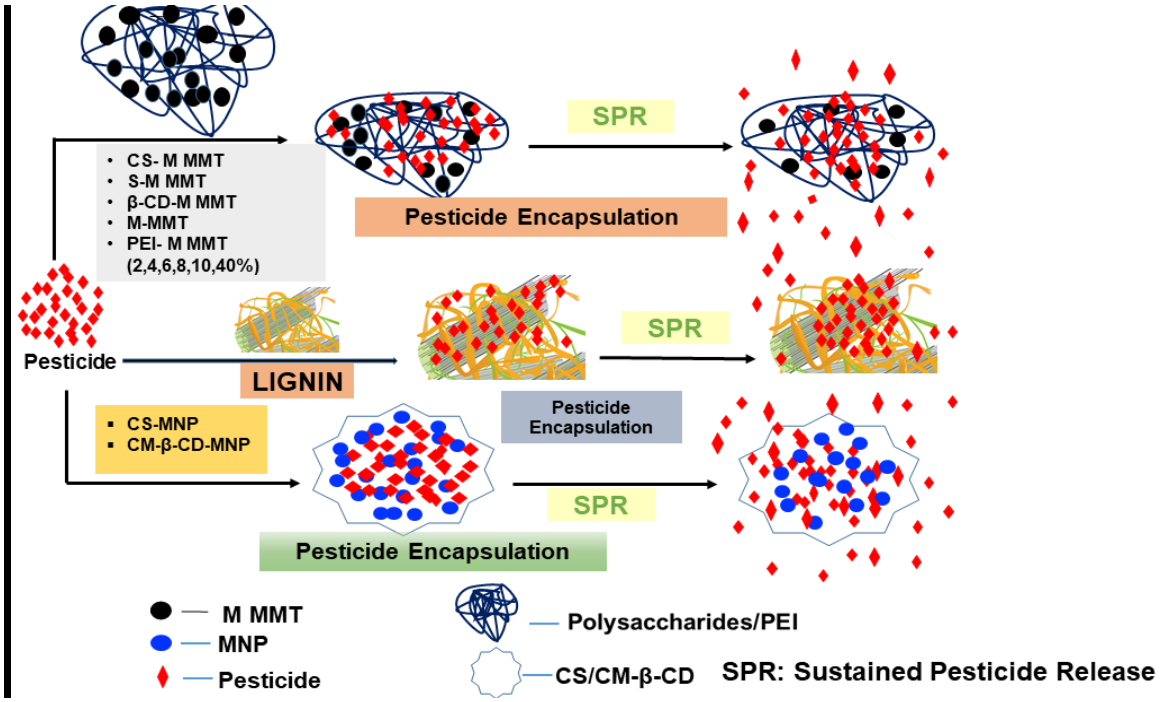

Figure 1. Types of system evaluated for pesticide encapsulation and release

In combination with nanotechnology, carbohydrates appear to be promising candidates for increasing E.E. We synthesized a sequence of hybrid M MMTs/MNPs of polysaccharides (chitosan,[20] starch [21] β-cyclodextrin[22] CM-β-cyclodextrin [23] lignin,[24] PEIs[25] forming hybrid nanocomposites by wet impregnation[27], gelation[28] and coprecipitation[29] in our attempt to further compare sustained pesticide release and enhanced E.E. methodologies (Figure 1). Compared with M MMT[26] PEI - M MMT[27] nanocomposites (2,4,6,8,10 & 40 %), CS-M MMT [28] S-M MMT, [29] β-CD-M MMT[30, 36] nanocomposites and L-M MMT[31] composites, the hybrid MNP NCs were designed as CS-MNP,[32] CM-β-CD-MNP [33]and compared with their EE % & PLE %age of chlorpyrifos. Finally, spectrophotometrically, sustained pesticide release (SPR) was determined wherein time-dependent release of chlorpyrifos from the above synthesized formulations was compared. (Figure 1). Because of its phenol groups, which are capable of scavenging free radicals,[34] Lignin was tried as it can serve as a stabilizer against UV

degradation or thermo-oxidation (Figure 1). Although the macro-to-nano-particles were discussed in a significant number of papers, it was shown that particle size reduction to nano shows pronounced E.E and SPR values due to more spaces (surface area) for insecticide molecules to be trapped. [35] Another main aim of this research is to figure out which is the better nanotechnology (MNP vs M MMT). This is the first systematic relative account of E.E %, PLE wt % and polysaccharides vs. lignin vs. PEI aqueous release activity of chlorpyrifos using M MMT/MNP nanomaterials.

2. EXPERIMENTAL SECTION

2.1 Materials and Reagents. Iron (III) chloride hexahydrate ($FeCl_3.6H_2O$); iron (II) chloride tetrahydrate ($FeCl_2.4H_2O$); ferric nitrate, ferrous sulfate**,** Montmorillonite (MMT), Polyethyleneimine (PEI), phosphate buffer Microcrystalline β-cyclodextrin (β-CD), Lignin(L), Chitosan (CS), chlorpyrifos (chp), were obtained from Sigma Aldrich. Starch (S), hydrochloric acid (HCl), sodium hydroxide (NaOH), Methanol (MeOH), acetic acid (AcOH), , ethanol (EtOH), , monochloroacetic acid, Acetone (Me_2CO) was obtained from Rankem. Dialyzer tubes (MWCO 1KDa) were procured from G-Biosciences. Carboxymethyl-β-cyclodextrin was synthesized from microcrystalline β-cyclodextrin as per literature procedure [36]

2.2 Analytical methods. X-ray Diffraction (XRD) was performed using Bruker D-8 advanced diffractometer in the 2θ range of 10 to 90 °C. The average crystallite size with and without surface coating was estimated using the Scherrer equation. Fourier transform infrared (FT–IR) spectra were recorded on Agilent Cary 660 spectrometer using the KBr pellet technique in a range of 4000–400 cm^{-1}. Thermogravimetric analysis (TGA) was performed to determine the degradation/decomposition behavior of samples using thermogravimetric (TG) analyzer-(Perkin Elmer STA 8000) at a N_2 flow rate of 10 mL/min and heating rate of 10 °C/min. Atomic Force Microscopy (AFM) images were acquired using Bruker Multimode 8 and sample analysis was done in tapping mode. The samples were deposited on silicon wafers and analysis was performed at different sections at room temperature and ambient atmosphere.

Transmission Electron microscopy (TEM) images were acquired on a Jeol 2100 HR operating at 200 kV. Samples were prepared by depositing a drop of diluted NP suspension on 300 mesh TEM grid were dried under vacuum for 2 h. Inductively coupled plasma-mass spectrometer (ICP-MS) was used to estimate the amount of iron for calculating mol% and turn over frequency (TOF), Agilent Technologies 7700 series.

The GC-MS analysis was performed to determine the encapsulation efficiency and pesticide loading efficiency using a Shimadzu GC coupled with a GCMS-QP 2010 plus mass detector and a single-quadrupole mass spectrometer Quantum (Shimadzu) with 100% dimethyl polysiloxane (Restek Rxi-1ms; 30 m × 0.25 mmiD., 0.25 μm film thickness) column. GC-MS operating conditions: The initial oven temperature was 60 °C, maintained for 1 min and then ramped to 270 °C at a rate of 10 °C/min followed by holding for 5 min at 270 °C. The initial temperature of the injector was 63 °C and then programmed at the same rate as the oven. Helium was used as carrier gas with primary pressure of 570 KPa. The split injection mode was used with a split ratio of 10.0. The injection volume of each sample was 1 μL and the total time for one GC-MS run was 27 min. Mass spectrometer settings: electron impact ionization mode with an electron energy of 70 eV, ion source and interface temperatures were set at 200 and 270 °C, respectively and scan mass range *m/z* 50–500. Shimadzu 2600 UV-Vis spectrophotometer was used to estimate the amount of entrapped pesticide at 214 nm during the aqueous release study after every 24 h. The calibration curve of ChP was prepared in MeOH.

2.3 Synthesis of Polysaccharide - Modified MMT/ Modified MMT/ Polysaccharide – MNP, Lignin - Modified MMT Nanocomposites, Polyethyleneimineimine- Modified MMT as pesticide nanocarriers (NCs)

Various hybrid materials were developed and synthesized in this research (Scheme 1). Hybrid NC containing polysaccharides, such as (CS-M MMT, S-M MMT and β-CD-M MMT), polyethyleneimine (PEI) such as PEI-M MMT (2,4,6,8,10 & 40%), MNP (such as CS-MNP,

CM-β-CD-MNP, lignin, such as L-M MMT, and inorganic nanofillers, such as modified MMT (M MMT). The M MMTs were used as filler or stabilizer with polysaccharides, lignin, PEI while polysaccharides were used as capping agents to prepare smaller sized polysaccharide/MNPs nanocomposites.(Scheme 1).

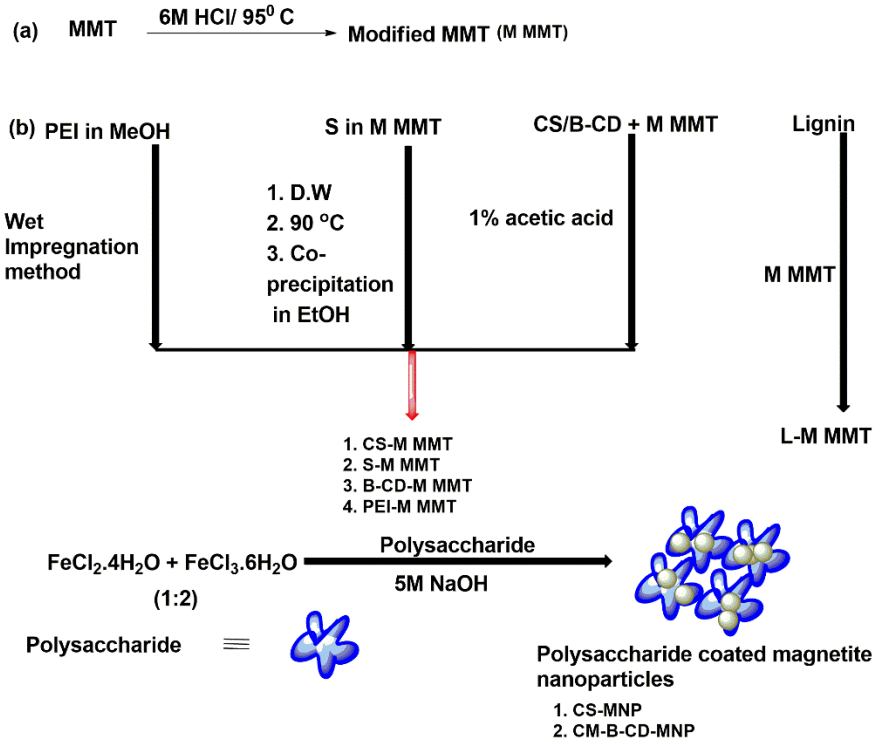

Scheme 1. : Synthesis of M MMT/ Polysaccharide- M MMT / Lignin- M MMT/ PEI- M MMT and Polysaccharide-MNP as Pesticide encapsulation and carrier.

In this study, the synthesis of Chlorpyrifos loaded nanocarriers involves two stages (Scheme 1).

i. Synthesis of modified montmorillonite (M MMT) / PEI- M MT/Polysaccharide- M MMTs / Polysaccharide-MNPs/ Lignin- M MMT

ii. Synthesis of chlorpyrifos loaded modified montmorillonite (M MMT) / PEI- M MT/Polysaccharide- M MMTs / Polysaccharide-MNPs/ Lignin- M MMT

2.3. (i)a: Synthesis of modified montmorillonite (M MMT) by acid treatment

The synthesis of modified montmorillonite was adapted from the literature with minor changes to improve textural properties, especially pore volume and surface area of clay samples.[37] 2g of clay was added to a 20ml solution of 6M hydrochloric acid. The mixture was then heated for 4 hours in an oil bath at 95°C while stirring at 600 rpm. The suspension was then washed with distilled water before being dried overnight in a 100°C oven. The powder was vacuum-dried for another 24 hours before application.

2.3. (i)b: Preparation of the PEI-M MMT nanocomposite

Approximately 2 g of PEI was dissolved in 20 g of methanol for 30 minutes while stirring. Wet impregnation method was used to make the PEI-M MMT composite sorbents, which was adapted from the literature with slight changes.[37] The M MMT was then added to the above-mentioned methanol solution and stirred at room temperature for 3h. The slurry was then dried for 12h at 75^0 C in a vacuum oven. PEI-M MMT samples with various PEI loadings of 2,4,6,8,10, and 40 wt percent were prepared to optimize the PEI loading on the M MMT.

2.3.(i)c: Preparation of Starch- M MMT nanocomposite

S-M MMT nanocomposite was synthesized by coprecipitation in ethanol as reported in the literature with minor modification.[38] 1g of starch was suspended in distilled water (100 ml) and heated at 100 ^{0}C for 30 min. An aqueous M MMT dispersion containing 0.12g of M MMT in 20 ml distilled water was slowly added to the starch solution. The mixture was stirred for 4 hours at 90°C. By applying 100ml of 95 % ethanol to the S-M MMT mixture and keeping it at 4 ^{0}C overnight, the S-M MMT mixture was precipitated. The precipitate was centrifuged for 5 min before being vacuum dried at 50 ^{0}C. To swell the starch molecule, the nanocomposites were blended with plasticizers (nanocomposites: water: glycerol = 100:40:30) in a speed mixer and held at room temperature for two days.

2.3. (i)d: Preparation of the CS-M MMT nanocomposite

With minor modifications, the preparation of the CS-M MMT nanocomposite was adapted from the literature[39]1 g of Chitosan was mixed with 1 percent acetic acid to make Chitosan solutions (100 mL). After 1 hour of stirring at 60 °C, the solutions were stirred continuously at room temperature overnight. NaOH was used to get the pH of the solution down to 4.9. 5g of well-dispersed M MMT suspension was prepared in 100ml of water and held at 60 °C overnight with stirring, then centrifuged to remove any solids. M MMT dispersions (100 mL) were combined with chitosan solutions for 1 day at 60°C. The mixture was centrifuged for 5 min. The supernatants, which had excess chitosan, were discarded after five washes with distilled water. After that, the solids were dried in a vacuum oven at 50 ^{0}C. [39]

2.3.(i)e: Preparation of the β-CD-M MMT nanocomposite

With minor modifications, the β-cyclodextrin -M MMT solution was synthesized according to the literature.[40] To produce a homogeneous mixture, β-cyclodextrin (1g) was dissolved in 25 ml acetic acid solution (1%) and stirred for 4 h. A suspension of 2% M MMT (500 mg) in acetic acid solution (1%, 25 ml) was also prepared. The suspension was added into the resulting gel. To produce a homogeneous β-CD-M MMT suspension, the mixture was stirred at 50°C for 2 days and then freeze dried.

2.3. (i)f: Preparation of the CM-β-CD-MNP

With minor modifications, CM-β-CD was synthesized as described in the literature.[41] A solution of 16.3 percent monochloroacetic acid (2.7 ml) was used to treat a mixture of β-CD (1 g) and NaOH (0.93 g) in water (3.7 ml) at 50 ^{0}C for 5 h. The pH values were modified in the range of 6–7 after the temperature of the reaction mixture was decreased to 25 °C. The obtained neutral

solution was mixed with 10 mL of methanol to create a white carboxymethylated-β-cyclodextrin precipitate, which was purified and dried in a 50 °C oven.

With minor modifications, CM-β-CD-MNP was synthesized according to published methods. [41] With rapid stirring at a speed of 1200 rpm, 0.57 g $FeCl_2.4H_2O$, 1.57 g $FeCl_3.6H_2O$, and 1 g CM-β-CD were dissolved in 26.7 ml distilled water. As the reaction mixture reached 90 °C, 3.5 mL liquid ammonia (25%) was added in drops. The reaction was held at 90 °C for 1 hour with continuous stirring. The nanoparticles were then washed in distilled water to eliminate any unreacted contaminants before being dried in a 70 °C oven.

2.3. (i)g: Preparation of the CS-MNP

The chitosan-coated MNP were made by in situ co-precipitation of iron salts, as described in the literature, but with a few tweaks [42]An amount of 3.6×10^{-3} moles of iron from a mixture in a molar ratio $2:1$ ($Fe^{3+}:Fe^{2+}$) of ferric nitrate (3.19g) and ferrous sulfate (1.19g) added to chitosan (5g in 100ml) was mixed at 100 rpm in 3% (*v*/*v*) acetic acid(10ml) at 70°C. An ultrasonic processor was used to spread the chitosan-iron solution, allowing for smoother compound delivery. Following that, a solution of 20% (w/v) NaOH : 96 percent (v/v) ethanol in a 12:3 volume ratio was added to the produced chitosan iron solution to precipitate it (30ml). The alkaline mixture was then homogenized using a vortex for 30 seconds before being shaken gently (60 rpm) for 18 h. After centrifugation for 5 minutes, the precipitate was washed in a 1:1 volume ratio of 50 mM phosphate buffer pH 7.0 and 96 percent (v/v) ethanol before neutralized. The neutralized solids were dried in an oven at 80 °C for 5 hours before being pounded to a fine powder.

2.3.(i)h: Preparation of the L-MMT complex

Minor modifications were made to the L-M MMT complex, as stated in the literature. [43] 1 g

M MMT and 1 g lignin were suspended in 30 mL sterile water and stirred for 12 h at room temperature. The L-M MMT complex was centrifuged and dried in a 65 °C oven for 24 h for powder processing.

2.3. (ii) General procedure for loading of ChP into Polysaccharide-MNPs / Polysaccharide- M MMT/ PEI- M MMT / lignin-M MMT hybrid and inorganic(M MMT) carriers.

As discussed in my previous paper, a dropwise application of a methanolic (2 mL) solution of ChP (20 mg) to the modified montmorillonite (M MMT) / PEI- M MMT/Polysaccharide- M MMT/ Polysaccharide-MNPs/ Lignin- M MMT (90 mg) suspension in MeOH (10 mL) was agitated at 500 rpm for 3 h at 25 °C. (Figure 2). [44] With the aid of an external magnet, the ChP-loaded nanocarriers were collected, washed with methanol, and vacuum dried for 1 h at 37 °C. The supernatant was taken to determine the free and entrapped pesticide concentrations. (Figure 2).

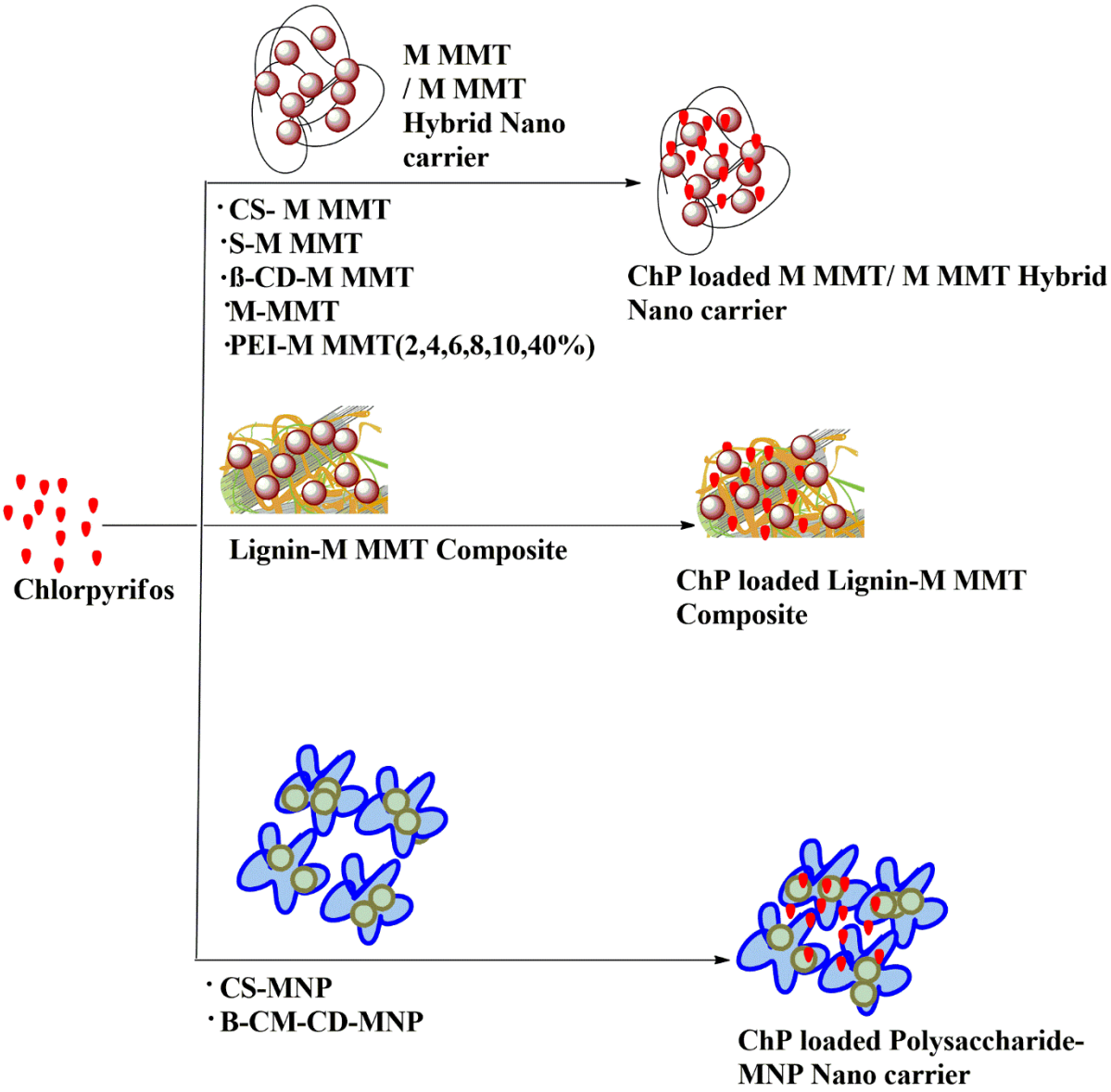

Figure 2. Synthesis of ChP loaded NCs.

2.4 Quantification of Pesticide Loading Efficiency (PLE) and Entrapment Efficiency (E.E). Using gas chromatography mass spectrometry (GC-MS) analysis with a retention period of 19.8 min, the amount of free pesticide present in the supernatant was measured (Section B in the SI). In MeOH, the calibration curve of ChP was prepared (Figure S12 & S13 in SI). Using the following equations, PLE (wt %) and E.E % were computed and the results are shown in Table S3 and S4 in SI .

$$\text{E. E\%} = \frac{\text{Amount of pesticide} - \text{Amount of free pesticide}}{\text{Total amount of particles}} \times 100 \qquad (1)$$

$$\text{PLE\%} = \frac{\text{Amount of pesticide} - \text{Amount of free pesticide}}{\text{Total amount of pesticide}} \times 100 \qquad (2)$$

2.4.a. The PLE and E.E values correction by ICP-MS for M MMT and hybrid NCs**.**

The pesticide loading study was carried out with the same volume for all the NCs (90 mg). Using ICP-MS (GC MS/ICP-MS data available in Section B3, B4, Table S3 in SI), the %age of iron oxide content present in hybrid NCs such as CS-MNP and CM-β-CD-MNP was calculated at 4.14 and 2.49 %, respectively.

2.5 Aqueous release behavior of ChP from hybrid and organic NCs.

Samples of PEI-M MMT / Polysaccharide-M MMT/ Polysaccharide-MNPs/L-M MMT hybrid and inorganic (M MMT) of known weights (20 mg) were placed in a glass vial containing 15 ml of phosphate buffer at pH 6.5 at ambient temperature for slow release studies of loaded Chp loaded NCs.[45] The set-up was gently shaken and the was weighed, pH was measured (Table S6 in SI) and 1 ml of the liquid was removed for examination and supplemented with a fresh 1 ml of the medium to preserve the sink state. After syringe-filtering the aliquot, a UV-Vis spectrometer was used to investigate the release and correlate the concentration emitted with the Chp calibration map.

Statistical analysis: All of the measurements were repeated at least three times (n = 3) to ensure that the results were repeatable, and the data were summarized as mean T s.d., with error bars shown in the data points in some of the figures.

3. RESULTS AND DISCUSSION

3.1. Synthesis of M MMT/ Polysaccharide-M MMT/ PEI-M MMT/ Polysaccharide-MNP and Lignin-M MMT as pesticide nanocarriers (NC)

We chose polysaccharides like Chitosan (CS), Starch (S), and β-Cyclodextrin (β-CD) for this analysis to compare polysaccharides like starch and cellulose NPs and MNPs described in our previous paper. The polysaccharide coating on MNP not only makes it more stable, but it also makes it less toxic, allowing the formulation to directly reach the target. We also contrasted it with M MMT, which works in the polymer matrix as nanofillers including polysaccharides, lignin, and PEI in the polymer matrix to significantly improve a range of physicochemical properties needed in new fields of application. As a result, in addition to comparing polysaccharides, lignin, and PEI, we also compare M MMT vs MNP encapsulation studies.

3.2 Characterization of M MMT and hybrid -materials. Studies using FT-IR, PXRD, TEM, AFM, TGA, Zeta, and DLS were conducted. In order to quantify the iron oxide content and properties, MNP hybrid nanocomposites were subjected to ICP-MS studies. The details are outlined below.

3.2.1 FT–IR analysis. Comparative FT-IR spectra of M MMT and hybrid NCs (PEI-M MMT (2%, 4%, 6%, 8%, 10%, 40%)/ CS-M MMT/S-M MMT/ β-CD-M MMT /L-M MMT/ CS-MNP/ CM-β-CD-MNP/) are shown in Figure 3a and 3b, respectively.

The inner surface OH peaks at 3620 cm^{-1} and 3697 cm^{-1}persisted in the spectrum of the M MMT. The shift in the OH absorption band from (3441 cm^{-1} to 3443 cm^{-1}, 1627 cm^{-1} to 1626 cm^{-1}, and the absence of the 3410 cm^{-1} band suggested that modification was achieved on this site. Protons attack the -OH groups in the clay layers during acid activation of M MMT, creating changes in the adsorption bands ascribed to the OH vibration and octahedral cations.

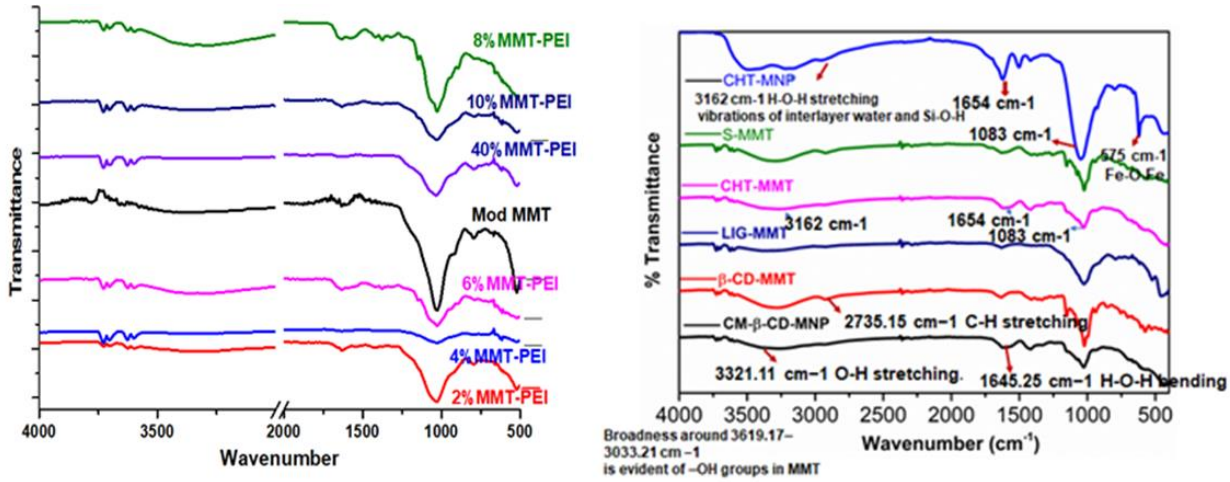

Figure 3. FT-IR spectra for the synthesized nanocomposites. (a) M MMT and Hybrid PEI-M MMT (b) Hybrid Polysaccharide - M MMT/ Polysaccharide-MNP/Lignin-M MMT nanocarrier.

Due to the bending vibration of the Si–O group, two peaks emerged at 1093 and 473 cm^{-1} in M MMT-PEI (2%, 4%, 6%, 8%, 10%, 40%) at varied loading quantities. The stretching vibration of $–CH_2$ in the PEI chain is responsible for the bands at 2850 and 2981 cm^{-1}. Two bands at 1590 and 1495 cm^{-1} were created by symmetric and asymmetric bending vibrations of –NH2, respectively, while another at 1660 cm^{-1} was attributed to asymmetric bending vibrations of $–NH_2$.

CS-M MMT NCs exhibit characteristic bands at 3627 cm^{-1} due to O–H stretching, a broad peak at 3449 cm^{-1} due to interlayer and intralayer H-bonded O–H stretching, 1641 cm^{-1} due to H–O–H bending, 1087 and 1035 cm^{-1} due to Si–O stretching, 916 and 626 cm^{-1} due to Al–OH, 843 and 793 cm^{-1} due to (Al, Mg)–OH vibration modes, and 520 and 467 cm^{-1} due to Si–O bending vibrations.

The spectrum of the S-M MMT reveals a mixture of absorptions due to the M MMT and the C-H starch stretching and bending groups. In S-M MMT, the C-H group peaks at 2988, 1425, and 1344 cm^{-1} in pure starch are moved to 2915, 1417, and 1350 cm^{-1}, corresponding to the deformation vibration of the C-H group of starch.

The peaks at 2928 cm^{-1} of β-CD-M MMT could be attributable to the methyl groups asymmetric stretching vibrations when compared to M MMT. In comparison to β-CD, the peaks at 1487 cm^{-1} of β-CD –M MT indicated the presence of CH2-N+ and might be assigned to NH3 +. Furthermore, a characteristic absorption peak of α-type glycosidic bond was discovered at 855 cm^{-1} of β-CD-M MMT, indicating that glucopyranose units generated β-CD via -1,4-glycosidic bond. Furthermore, when comparing M MMT to β-CD-M MMT, the peaks at 521 and 465 cm^{-1} can be attributable to Si-O-Al stretching and Si-O bending vibrations, respectively.

All MNP nanocomposites (CS-MNP/ CM-β-CD-MNP) showed a distinctive adsorption band of Fe–O bonds at 586 cm^{-1}, indicating the presence of iron oxide in the polymer matrix.

In CS-MNP, the band at 2,875 cm^{-1} was attributed to the symmetrical stretching of the -CH_2 group in the polymer, 1,660 cm^{-1} to the amide I group (C-O stretching along the N-H deformation), 1,557 cm^{-1} to the -NH deformation, 1,412 cm^{-1} to the C-N axial deformation (amine group), 1,374 cm^{-1} to the COO- group in carboxylic acid salt, and 1,157 cm^{-1} to peak of β (1-4) glucosidic bond.

The peak at 945 cm^{-1} in CM-β-CD-MNP is due to the R-1,4-bond skeleton vibration of β-CD The peak at 1704 cm^{-1} corresponds to carbonyl group (=CO) stretching, indicating that the carboxymethyl group (–$COOCH_3$) has been incorporated into the β-CD molecule. With a minor shift, all of the prominent peaks of CM-β-CD in the region of 900–1200 cm^{-1} are present in the spectrum of CM-β-CD-MNP. two peaks formed at 1623 and 1401 cm^{-1}, indicating that the COOH groups of CM-β-CD reacted with the surface OH groups of Fe3O4 particles, resulting in the creation of the iron carboxylate.

3.2.b. *Characterization by PXRD*: PXRD results have been depicted in Figure 4a-b. The characterized peak of M MMT [46]was observed at 2h = 6.9 corresponding to a basal spacing of

12.5 Å. Morphological characteristic of M MMT-PEI was assessed. As it can be seen, the graph shows the peaks of 7.3 and 6.5 at 2θ for MMT and MMT-PEI, respectively.

The diffraction peak of CS emerged at 2h = 10.7. After the incorporation of CS into M MMT, the obtained CS–M MMT nanocomposites exhibited a new peak at lowed angle of 5.8 while the intrinsic diffraction peak of M MMT disappeared, the absence of this peak in starch M MMT (5:1 and 10:1, w/w) indicated that the starch intercalated, exfoliated and adsorbed on the M MMT galleries to change the performance of clay galleries.

β-CD –M MMT[47] showed that after modification, the d_{001}-spacing was enlarged to 1.409 nm. It could be inferred that the modification may occur in the M MMT interlayer.

In L-M MMT, the diffractogram presents a good dispersion of the characteristic peaks of clay at 2θ = 5.8°, 8.8°, 12.2°, 17.4°, 19°, 35° and 62° which is attributed to T-O-T structure of M MMT.

The composite of CS-MNP shows a small broad peak at 19.80 was assigned to CS. The other diffraction peaks at 30.10, 35.50, 43.30 , 53.80 , 57.20 , 63.00 , and 74.80 were assigned to the (220), (311), (400), (422), (511), (440), and (533) planes of Fe_3O_4.

CM-β-CD–MNP indicate six characteristic peaks at 2 = 30.2◦, 35.6◦, 43.2◦, 53.7◦, 57.2◦, and 62.9◦. They relate to their corresponding indices (2 2 0), (3 1 1), (4 0 0), (4 2 2), (5 1 1), and (4 4 0), respectively. The crystal sizes of CM-β-CD–MNP determined from the XRD pattern by using Scherrer's equation are found to be 10.2 and 10.7 nm, respectively,

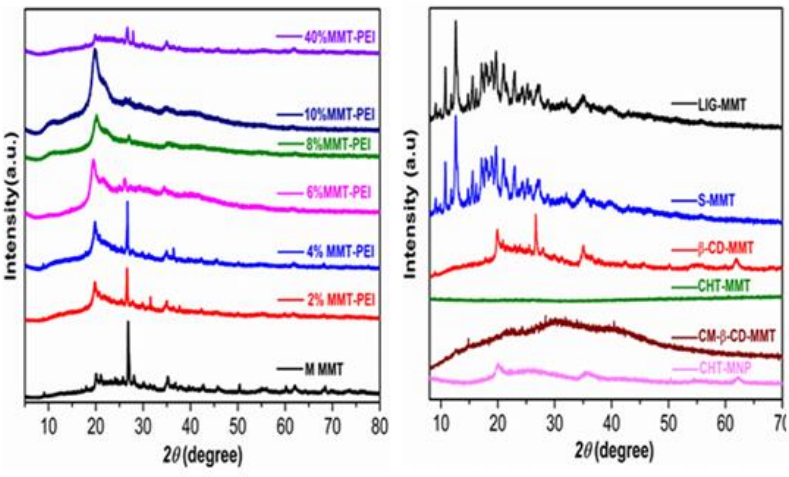

Figure 4. PXRD pattern for the synthesized nanocomposites. (a) M MMT and Hybrid PEI-M MMT (b) Hybrid Polysaccharide- M MMT/ Polysaccharide-MNP/Lignin-M MMT nanocarrier.

3.2 c. Particles Size analysis by TEM: The TEM images of M MMT reveal the internal structures of M MMT. It was observed that the layered crystallites of modified MMT aggregated in large sized particles. (Figure5a & b).

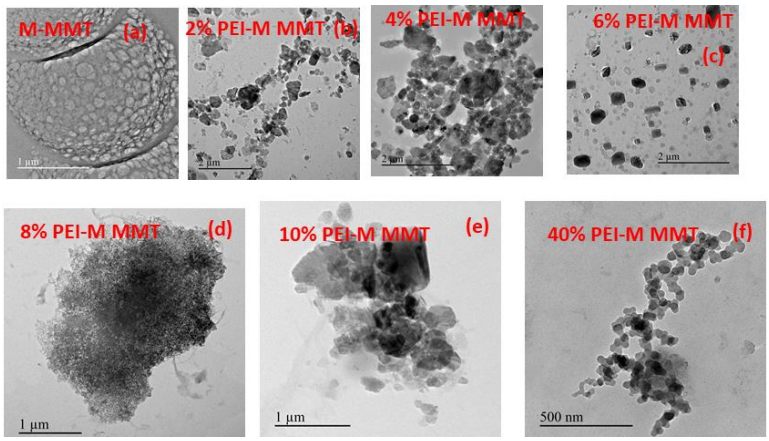

Figure 5. TEM images for the synthesized nanocomposites. (a) M MMT (b) 2% PEI-M MMT (c) 4 % PEI-M MMT (d). 6% PEI-M MMT (e) 8%Hybrid PEI-M MMT (f) 10%Hybrid PEI-M MMT (g) 40%Hybrid PEI-M MMT nanocarrier.

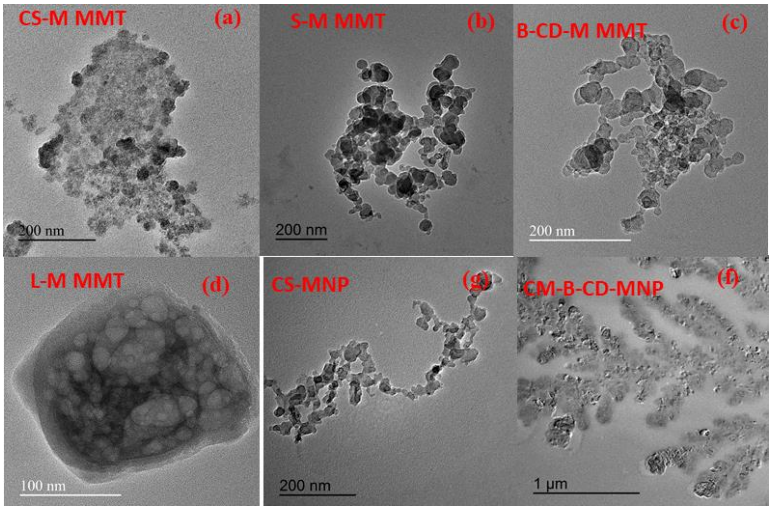

Figure 5. (b) TEM images of (a). CS-M MMT (b). S-M MMT (c). β-CD-M MMT (d) L-M MMT (e) CS-MNP (f). CM-β-CD-MNP nanocarrier.

The micrographs of PEI-M MMT composites clearly reveal that many clusters/stacks of M MMT platelets are seen in addition to finely dispersed M MMT. CS-M MMT shows the dark lines/platelets represent clay tactoids while the grey base corresponds to the chitosan matrix. For the S-M MMT nanocomposites, the clay platelets are poorly dispersed and form aggregates that break upon loading. In β-CD-MMT, showed very good clay dispersion with uniform distribution of silicate layers, leading to exfoliation morphology.

The particle size of L-M MMT[48]remained almost suggesting no aggregation in this complex. CS-MNP shows that MNP nanoparticles coated on the CS surface with an almost uniform distribution. Dark areas in the composite correspond to the crystalline MNP nanoparticles, whereas bright areas represent the amorphous CS.

In CM β-CD–MNP, well-shaped spherical or ellipsoidal magnetic nanoparticles are observed. (TableS1, S2 and Figure S1 & S2 in SI).

3.2. d. AFM.*Analysis* To investigate the effect of PEI, Polysaccharide and lignin loading onto the M MMT, the Polysaccharide capping on MNP, the morphology were investigated by AFM. (Figure S3 & S4 in SI). The digital morphology of the compounds was depicted in Figure S5 & S6 in SI.

3.2.e. *TGA Analysis:* The thermal stability of M MMT and PEI- M MMT with different PEI loading amounts were investigated and the weight loss as a function of temperature is shown in Fig. S7(a & b).

3.2f. *Zeta potential* The average zeta potential of the M MMTs and MNPs was 18.67mV and 27.55mV with conductivity of 0.045 and 0.8845 respectively. It is worth mentioning that the zeta potential for hybrid PEI-M MMT was higher than Polysaccharide-M MMTs/MNPs/Lignin-M MMT. (Figure S8 and S9 in SI).

3.2g. *DLS*: DLS showed the size range for M MMTs/MNP, MNPs in the range of -228.9 to 3728 d-nm material absorption, material RI and viscosity of 0.00, 1.47 and 1.8872 respectively The DLS was measured using water as dispersant with RI of 1.330 at 25^0C. (Figure S10 and S11 in SI).

3.3 Comparison of PLE and E.E for M MMT and hybrid-NCs.

After efficient loading of chlorpyrifos (chp) pesticide on the M MMTs/hybrid MMTs and hybrid MNPs, pesticide loading efficiency (PLE, wt %)) and encapsulation efficiency (E.E %) were quantified using gas chromatography-mass spectrometry (GC-MS) study and corrected with inductively coupled plasma mass spectrometry (ICP MS). (Table 1, Table S3, S4 in SI).

Table 1: Comparison of E.E% and PLE% of hybrid- M MMTs/MNPs

[a] E.E and PLE obtained from GC-MS (Table S1) including MNP part, [b] In case of hybrid NCs correction was applied by replacing the inorganic content to organic using ICP-MS (the calculation is provided in Section B3, SI. [c] Relative PLE with respect to L-M MMT= corrected PLE of (other sorbents / L-M MMT) *100.

Types of NC/ MMMT	NC	M mol	mg	E.E (%)[a]	PLE (%)[a]	Corrected E.E(%)[b]	Corrected PLE (wt %)[b]	Relative PLE[c]
Inorganic	M MMT	28.87	10.12	11.0	49.4	11.0	49.4	50.64
PEI-M MMT	2% PEI-M MMT	22.01	7.71	13.6	61.5	13.6	61.5	63.04
	4% PEI-M MMT	21.54	7.55	13.8	62.3	13.8	62.3	63.86
	6% PEI-M MMT	20.61	7.22	14.2	63.9	14.2	63.9	65.50
	8% PEI-M MMT	19.67	6.89	14.6	65.5	14.6	65.5	67.14
	10% PEI-M MMT	19.3	6.76	14.7	66.2	14.7	66.2	67.86
	40%PEI- M MMT	13.89	4.86	16.8	75.7	16.8	75.7	77.60
Polysaccharide-M MMT	CS-M MMT	28.40	9.95	11.2	50.3	11.2	50.3	51.56
	S-M MMT	11.22	3.93	17.8	80.4	17.8	80.4	82.41
	β-CD-M MMT	16.12	5.65	15.9	71.7	15.9	71.7	73.50
Lignin-M MMT	L-M MMT	1.41	0.49	21.6	97.55	21.6	97.55	100
Polysaccharide-MNP	CS-MNP	16.00	5.60	16	72	16.7	75.11	77
	CM-β-CD-MNP	16.85	5.90	15.7	70.5	16.10	72.30	74.12

Overall, with the corrected E.E and PLE values ranging between 11.0-21.6 % and 49.4-97.55wt % respectively, almost all sorbents have shown successful ChP entrapment. Several observations showed a comparison of corrected PLE values, i) hybrid macroscopic sorbent L-M MMT (97.55wt%) and S-M MMT (80.4wt%) showed substantially better performance than the corresponding inorganic M M MMT (49.4wt%) and CS-M MMT (50.3wt%). For L-M MMT, which showed surprisingly high PLE, this is particularly true. (ii) MNPs demonstrated higher PLE than M MMTs among the M MMTs and hybrid MNP NCs (CM-β-CD-MNP: 72.30; β-CD-M MMT: 71.7; CS-MNP: 75.11; CS-M MMT: 50.3).

These findings show that while slight alternation was found in terms of PLE, the PLE value was not greatly improved by functionalization. iii) CS-MNP outperforms β-CD-MNP among the hybrid NCs. Based on these findings, we infer that due to 1,4- & 1,6-linkages of the glucose unit, the high output of MNP over M MMT and better performance of S-M MMT may be attributed to the branching nature of starch, generating more space for pesticide packing.

3.4 In-vitro aqueous release behavior of nanocarriers.

Based on the absorption of ChP monitored using UV/Vis spectroscopy, time-dependent pesticide release concentration profiles were determined with the initial measurement of pH(Table S6 in SI). The release profiles of hybrid- M MMTs/ MNPs nanocarriers are shown in figures 9a and b. S-M MMT provided the best results for the following compounds tested (98 % in 12 days). However, Lignin-M MMT had strong E.E/PLE performance, but in 2 days the aqueous release behavior was only 3.5 %. While the other M MMT-Polysaccharide gave intermediate results. Of the MNPs, the CS-MNP gave comparatively better performance. (Table 2). However, as we increase the organic content, i.e. PEI, in M MMT-PEIs, the SPR results improve (40 % M MMT-PEI; 81 % in 10days while 2 % M MMT-PEI ; 65 % in 11 days). (Table 2, Figure 6a & b).

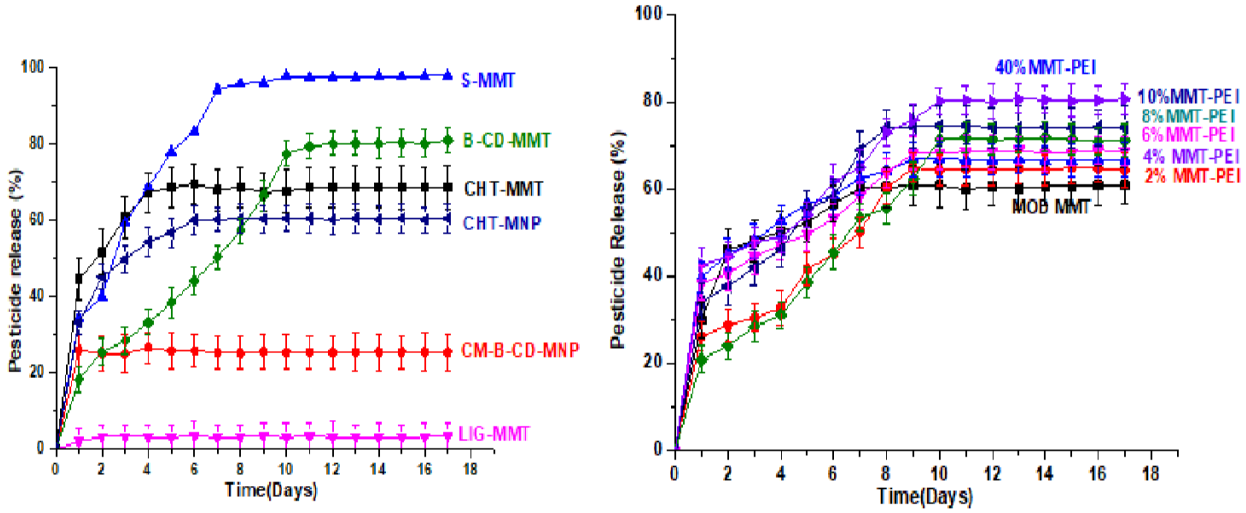

Figure 6. Aqueous release behavior of chlorpyrifos for the synthesized nanocomposites. Hybrid Polysaccharide-MNP/Lignin-M MMT/ Hybrid Polysaccharide-M MMT (B). M MMT. Hybrid MMT-PEI.

Table 2. Aqueous release behavior of chlorpyrifos for the synthesized inorganic NC and nanocomposites. (Hybrid Polysaccharide-MNP/Lignin-M MMT/ Hybrid Polysaccharide-M MMT (B). M MMT. Hybrid MMT-PEI).

S.NO	M MMT/Hybrid nanocomposites	Days	% Pesticide Release
1.	S-M MMT	12	98
2.	CD- M MMT	12	80
3.	CS- M MMT	09	67
4.	L- M MMT	02	3.5
5.	CS-MNP	06	60
6.	CM-β-CD-MNP	05	26
7.	M MMT	14	61
8.	2% PEI-M MMT	11	65
9.	4% PEI-M MMT	11	65
10.	6% PEI-M MMT	11	69
11.	8% PEI-M MMT	10	71
12.	10% PEI-M MMT	09	75
13.	40% PEI-M MMT	10	81

CONCLUSIONS

We systematically designed, synthesized and characterized the inorganic M MMT/ PEI-M MMTs(having different concentrations of PEIs.(2%, 4%, 6%, 8%, 10%, 40%)/ Polysaccharide-M MMT/ Polysaccharide-MNPs/ Lignin-M MMT in order to discern the role of inorganic support used in the hybrid materials and the type of materials synthesized such as M MMTs vs MNPs systems for pesticide delivery. Our study has unraveled the answers for these questions. Although, Lignin-M MMT had good E.E/PLE results, but SPR is only 3.5% in 2days and therefore not suitable for aqueous release studies. In M MMT-PEIs, as we increase the organic content (PEI), the SPR results improve (40% M MMT-PEI: 81% in 10days while 2% M MMT-PEI: 65% in 11 days). S-M MMT showed significantly better performance(80.4wt%) in comparison to all other polysaccharides Among the M MMTs and hybrid MNP NCs, MNPs exhibited higher PLE than M MMTs (CM-β-CD-MNP: 72.30; β-CD-M MMT: 71.7; CS-MNP: 75.11; CS-M MMT: 50.3). Among the hybrid NCs, CS-MNP has outperformed over β-CD-MNP. Based on these results, we infer that the high performance of MNP over M MMT and

better performance of S-M MMT that may be attributed to the branching nature of starch due to 1,4- & 1,6-linkages of glucose unit generate more rooms for the loading of the pesticide.

Supporting Information.

AUTHOR INFROMATION

Corresponding Author

ORCID

Ritu Mahajan: 0000-0002-6441-411X

Notes

The author declares no competing financial interest.

ACKNOWLEDGMENTS

This work was supported by the Department of Science and Technology (DST), Grant No. SR/WOS-B/818/2016 (G). RM thank for WOS-B Fellowship. The author thanks Institute of Nano Science and Technology for all facilities and Punjab Biotechnology Incubator for ICP-MS measurements.

ABBREVIATIONS

MMT, montmorillonite; M MMT, modified montmorillonite; L, lignin; CS, chitosan, S, starch; β-CD, β-cyclodextrin; PEI, polyethyleneimine; CM-β-CD, carboxymethyl-β-cyclodextrin; MNP, magnetite; PLE, pesticide loading efficiency; SPR, sustained pesticide release; Chp, Chlorpyrifos; GC-MS, gas chromatography-mass spectrometry; ICP MS, Inductively Coupled Plasma Mass Spectrometry; NPs, nanoparticles; E.E, encapsulation efficiency; $FeCl_3.6H_2O$, Iron (III) chloride hexahydrate; $FeCl_3.6H_2O$, iron (II) chloride tetrahydrate; NaOH, sodium hydroxide; HCl, hydrochloric acid; MeOH, methanol; AcOH, acetic acid; EtOH, ethanol;

Me_2CO, acetone; XRD, X-ray Diffraction; FT-IR, fourier transform infrared spectra; TGA, thermogravimetric analysis; AFM, atomic Force Microscopy; TEM, Transmission Electron microscopy; NC, nanocarrier; Fe_3O_4, magnetite.

REFERENCES

(1.). Shang, Y., Hasan, M. K., Ahammed, G. J., Li, M., Yin, H., & Zhou, J. (**2019**). Applications of Nanotechnology in Plant Growth and Crop Protection: A Review. Molecules, 24(14), 2558. doi:10.3390/molecules24142558.

(2). Kim, D.-Y., Kadam, A., Shinde, S., Saratale, R. G., Patra, J., & Ghodake, G. (**2017**). Recent developments in nanotechnology transforming the agricultural sector: a transition replete with opportunities. Journal of the Science of Food and Agriculture, 98(3), 849–864. doi:10.1002/jsfa.8749.

(3.). Fraceto, L. F., Grillo, R., de Medeiros, G. A., Scognamiglio, V., Rea, G., & Bartolucci, C. (**2016**). Nanotechnology in Agriculture: Which Innovation Potential Does It Have? Frontiers in Environmental Science, 4. doi:10.3389/fenvs.2016.00020.

(4). Kumar, S., Nehra, M., Dilbaghi, N., Marrazza, G., Hassan, A. A., & Kim, K.-H. (**2018**). Nano-based smart pesticide formulations: Emerging opportunities for agriculture. Journal of Controlled Release. doi:10.1016/j.jconrel.2018.12.012.

(5). Shang, Y., Hasan, M. K., Ahammed, G. J., Li, M., Yin, H., & Zhou, J. (**2019**). Applications of Nanotechnology in Plant Growth and Crop Protection: A Review. Molecules, 24(14), 2558. doi:10.3390/molecules24142558.

(6). de Jong. (**2008**). Drug delivery and nanoparticles: Applications and hazards. International Journal of Nanomedicine, 133. doi:10.2147/ijn.s596.

(7). Deng, Y., Zhang, X., Shen, H., He, Q., Wu, Z., Liao, W., & Yuan, M. (**2020**). Application of the Nano-Drug Delivery System in Treatment of Cardiovascular Diseases. Frontiers in Bioengineering and Biotechnology, 7. doi:10.3389/fbioe.2019.00489.

(8). Chivrac, F., Pollet, E., & Avérous, L. (**2009**). Progress in nano-biocomposites based on polysaccharides and nanoclays. Materials Science and Engineering: R: Reports, 67(1), 1–17. doi:10.1016/j.mser.2009.09.002.

(9). Guo, F., Aryana, S., Han, Y., & Jiao, Y. (**2018**). A Review of the Synthesis and Applications of Polymer–Nanoclay Composites. Applied Sciences, 8(9), 1696. doi:10.3390/app8091696.

(10). Mittal, V. (**2009**). Polymer Layered Silicate Nanocomposites: A Review. Materials, 2(3), 992–1057. doi:10.3390/ma2030992.

(11). Nilsen, O., Foss, S., Kjekshus, A., & Fjellvåg, H. (**2008**). Growth of Nano-Needles of Manganese(IV) Oxide by Atomic Layer Deposition. Journal of Nanoscience and Nanotechnology, 8(2), 1003–1011. doi:10.1166/jnn.2008.037.

(12). Pavlidou, S., & Papaspyrides, C. D. (**2008**). A review on polymer–layered silicate nanocomposites. Progress in Polymer Science, 33(12), 1119–1198. doi:10.1016/j.progpolymsci.2008.07.008.

(13). Singh, D., McMillan, J. M., Liu, X.-M., Vishwasrao, H. M., Kabanov, A. V., Sokolsky-Papkov, M., & Gendelman, H. E. (**2014**). Formulation design facilitates magnetic nanoparticle delivery to diseased cells and tissues. Nanomedicine, 9(3), 469–485. doi:10.2217/nnm.14.4.

(14). Fu, S.-Y., Sun, Z., Huang, P., Li, Y.-Q., & Hu, N. (**2019**). Some basic aspects of polymer nanocomposites: A critical review. Nano Materials Science. doi:10.1016/j.nanoms.2019.02.006.

(15). Dantas de Oliveira, A., & Augusto Gonçalves Beatrice, C. (**2019**). Polymer Nanocomposites with Different Types of Nanofiller. Nanocomposites - Recent Evolutions. doi:10.5772/intechopen.81329.

(16). Mohammed, L., Ansari, M. N. M., Pua, G., Jawaid, M., & Islam, M. S. (**2015**). A Review on Natural Fiber Reinforced Polymer Composite and Its Applications. International Journal of Polymer Science, 2015, 1–15. doi:10.1155/2015/243947.

(17). Mhd Haniffa, M., Ching, Y., Abdullah, L., Poh, S., & Chuah, C. (**2016**). Review of Bionanocomposite Coating Films and Their Applications. Polymers, 8(7), 246. doi:10.3390/polym8070246.

(18). Mishra, R. K., Sabu, A., & Tiwari, S. K. (**2018**). Materials chemistry and the futurist eco-friendly applications of nanocellulose: Status and prospect. Journal of Saudi Chemical Society. doi:10.1016/j.jscs.2018.02.005.

(19). Varma, R. S., & Iravani, S. (**2020**). Greener synthesis of lignin nanoparticles and their applications. Green Chemistry. doi:10.1039/c9gc02835h.

(20). Li, Jianfa; Yao, Jian; Li, Yimin; Shao, Ying (2012). Controlled release and retarded leaching of pesticides by encapsulating in carboxymethyl chitosan /bentonite composite gel. Journal of Environmental Science and Health, Part B, 47(8), 795–803. doi:10.1080/03601234.2012.676421

(21). Ihegwuagu, N. E., Sha'Ato, R., Tor-Anyiin, T. A., Nnamonu, L. A., Buekes, P., Sone, B., & Maaza, M. (**2016**). Facile formulation of starch–silver-nanoparticle encapsulated dichlorvos and chlorpyrifos for enhanced insecticide delivery. New Journal of Chemistry, 40(2), 1777–1784. doi:10.1039/c5nj01831e.

(22). Campos, E. V. R., Proença, P. L. F., Oliveira, J. L., Melville, C. C., Della Vechia, J. F., de Andrade, D. J., & Fraceto, L. F. (**2018**). Chitosan nanoparticles functionalized with β-cyclodextrin: a promising carrier for botanical pesticides. Scientific Reports, 8(1). doi:10.1038/s41598-018-20602-y.

(23). Badruddoza, A. Z. M., Tay, A. S. H., Tan, P. Y., Hidajat, K., & Uddin, M. S. (**2011**). Carboxymethyl-β-cyclodextrin conjugated magnetic nanoparticles as nano-adsorbents for removal of copper ions: Synthesis and adsorption studies. Journal of Hazardous Materials, 185(2-3), 1177–1186. doi:10.1016/j.jhazmat.2010.10.029.

(24). Lu, Y., Lu, Y.-C., Hu, H.-Q., Xie, F.-J., Wei, X.-Y., & Fan, X. (**2017**). Structural Characterization of Lignin and Its Degradation Products with Spectroscopic Methods. Journal of Spectroscopy, 2017, 1–15. doi:10.1155/2017/8951658.

(25). Larraza, I., López-Gónzalez, M., Corrales, T., & Marcelo, G. (**2012**). Hybrid materials: Magnetite–Polyethylenimine–Montmorillonite, as magnetic adsorbents for Cr(VI) water treatment. Journal of Colloid and Interface Science, 385(1), 24–33. doi:10.1016/j.jcis.2012.06.050.

(26). Al-Samhan, M., Samuel, J., Al-Attar, F., & Abraham, G. (**2017**). Comparative Effects of MMT Clay Modified with Two Different Cationic Surfactants on the Thermal and Rheological Properties of Polypropylene Nanocomposites. International Journal of Polymer Science, 2017, 1–8. doi:10.1155/2017/5717968.

(27). Zhang, C., Oliaee, S. N., Hwang, S. Y., Kong, X., & Peng, Z. (**2015**). A Generic Wet Impregnation Method for Preparing Substrate-Supported Platinum Group Metal and Alloy Nanoparticles with Controlled Particle Morphology. Nano Letters, 16(1), 164–169. doi:10.1021/acs.nanolett.5b04518.

(28). Pedroso-Santana, S., & Fleitas-Salazar, N. (**2020**). Ionotropic gelation method in the synthesis of nanoparticles/microparticles for biomedical purposes. Polymer International. doi:10.1002/pi.5970.

(29). Peternele, W. S., Monge Fuentes, V., Fascineli, M. L., Rodrigues da Silva, J., Silva, R. C., Lucci, C. M., & Bentes de Azevedo, R. (**2014**). Experimental Investigation of the Coprecipitation Method: An Approach to Obtain Magnetite and Maghemite Nanoparticles with Improved Properties. Journal of Nanomaterials, 2014, 1–10. doi:10.1155/2014/682985.

(30). Zeng, A., & Zeng, A. (**2017**). Synthesis of a Quaternized Beta Cyclodextrin-Montmorillonite Composite and Its Adsorption Capacity for Cr(VI), Methyl Orange, and p-Nitrophenol. Water, Air, & Soil Pollution, 228(8). doi:10.1007/s11270-017-3461-y.

(31). Tahari, Nadia; de Hoyos-Martinez, Pedro L.; Abderrabba, Manef; Ayadi, Sameh; Labidi, Jalel (2020). Lignin - montmorillonite hydrogels as toluene adsorbent. Colloids and Surfaces A: Physicochemical and Engineering Aspects, (), 125108–. doi:10.1016/j.colsurfa.2020.125108

(32). El Zowalaty, M., Webster, T. J., Zobir Hussein, M., Ismail, M., & Hussein-Al-Ali, S. (**2014**). Synthesis, characterization, controlled release, and antibacterial studies of a novel streptomycin chitosan magnetic nanoantibiotic. International Journal of Nanomedicine, 549. doi:10.2147/ijn.s53079.

(33). Li, Hongguang; El-Dakdouki, Mohammad H.; Zhu, David C.; Abela, George S.; Huang, Xuefei (2012). Synthesis of β-cyclodextrin conjugated superparamagnetic iron oxide nanoparticles for selective binding and detection of cholesterol crystals. Chemical Communications, 48(28), 3385–. doi:10.1039/C2CC17852D.

(34). (35). Gregorová, A., Cibulková, Z., Košíková, B., & Šimon, P. (**2005**). Stabilization effect of lignin in polypropylene and recycled polypropylene. Polymer Degradation and Stability, 89(3), 553–558. doi:10.1016/j.polymdegradstab.2005.02.007.

(35). 36). Huang, B., Chen, F., Shen, Y., Qian, K., Wang, Y., Sun, C., … Cui, H. (**2018**). Advances in Targeted Pesticides with Environmentally Responsive Controlled Release by Nanotechnology. Nanomaterials, 8(2), 102. doi:10.3390/nano8020102.

(36). Pellicer, JosÃ© A.; RodrÃguez-LÃ³pez, MarÃa Isabel; Fortea, MarÃa Isabel; GÃ³mez-LÃ³pez, Vicente M.; AuÃ±Ã³n, David; NÃºÃ±ez-Delicado, Estrella; GabaldÃ³n, JosÃ© A. (2020). Synthesis of New Cyclodextrin-Based Adsorbents to Remove Direct Red 83:1. Polymers, 12(9), 1880–. doi:10.3390/polym12091880

(37). Acisli, Ozkan; Khataee, Alireza; Karaca, Semra; Sheydaei, Mohsen (2016). Modification of nanosized natural montmorillonite for ultrasound-enhanced adsorption of Acid Red 17. Ultrasonics Sonochemistry, 31(), 116–121. doi:10.1016/j.ultsonch.2015.12.012

(38). Chung, Y.-L., Ansari, S., Estevez, L., Hayrapetyan, S., Giannelis, E. P., & Lai, H.-M. (**2010**). Preparation and properties of biodegradable starch–clay nanocomposites. Carbohydrate Polymers, 79(2), 391–396. doi:10.1016/j.carbpol.2009.08.021.

(39). Günister, E., Pestreli, D., Ünlü, C. H., Atıcı, O., & Güngör, N. (**2007**). Synthesis and characterization of chitosan-MMT biocomposite systems. Carbohydrate Polymers, 67(3), 358–365. doi:10.1016/j.carbpol.2006.06.004.

(40). Ding, Wen-Ya; Zheng, Si-Di; Qin, Yue; Yu, Fei; Bai, Jing-Wen; Cui, Wen-Qiang; Yu, Tao; Chen, Xing-Ru; Bello-Onaghise, God'spower; Li, Yan-Hua (2019). Chitosan Grafted With β-Cyclodextrin: Synthesis, Characterization, Antimicrobial Activity, and Role as

Absorbefacient and Solubilizer. Frontiers in Chemistry, 6(), 657–. doi:10.3389/fchem.2018.00657

(41). Zeinali S, Abdollahi M, Sabbaghi S, Carboxymethyl-β-cyclodextrin Modified Magnetic Nanoparticles for Effective Removal of Arsenic from Drinking Water: Synthesis and Adsorption Studies. J. Water Environ. Nanotechnol., **2016**;1(2):104-115. DOI: 10.7508/jwent.2016.02.004.

(42).). Díaz-Hernández, A., Gracida, J., García-Almendárez, B. E., Regalado, C., Núñez, R., & Amaro-Reyes, A. (**2018**). Characterization of Magnetic Nanoparticles Coated with Chitosan: A Potential Approach for Enzyme Immobilization. Journal of Nanomaterials, 2018, 1–11. doi:10.1155/2018/9468574.

(43). Peng, Y., Wang, W., & Cao, J. (**2016**). Preparation of Lignin–Clay Complexes and Its Effects on Properties and Weatherability of Wood Flour/Polypropylene Composites. Industrial & Engineering Chemistry Research, 55(36), 9657–9666. doi:10.1021/acs.iecr.6b02660.

(44). Ritu Mahajan,[!] Abdul Selim,[!] Vijayakumar Shanmugam, Govindasamy Jayamurugan*
A Methodical Study to Unravel the Potential of using Polysaccharides based Organic Nanoparticles Versus Hybrid Nanoparticles for Pesticide Delivery, self-archived on 22nd January 2021 to the preprint version of ChemRxiv (DOI: https://doi.org/10.26434/chemrxiv.13619486.v1).

(45). Yang, Feng-Lian; Li, Xue-Gang; Zhu, Fen; Lei, Chao-Liang (2009). Structural Characterization of Nanoparticles Loaded with Garlic Essential Oil and Their Insecticidal Activity against Tribolium castaneum (Herbst) (Coleoptera: Tenebrionidae). Journal of Agricultural and Food Chemistry, 57(21), 10156–10162. doi:10.1021/jf9023118

(46). Alshabanat, Mashael; Al-Arrash, Amal; Mekhamer, Waffa (2013). Polystyrene/Montmorillonite Nanocomposites: Study of the Morphology and Effects of Sonication Time on Thermal Stability. Journal of Nanomaterials, 2013(), 1–12. doi:10.1155/2013/650725

(47). Mahmood, Asif; Sharif, Amara; Muhammad, Faqir; Sarfraz, Rai Muhammad; Abrar, Muhammad Asad; Qaisar, Muhammad Naeem; Anwar, Naveed; Amjad, Muhammad Wahab; Zaman, Muhammad (2019). Development and in vitro evaluation of (β-cyclodextrin-g-methacrylic acid)/Na⁺-montmorillonite nanocomposite hydrogels for controlled delivery of lovastatin . International Journal of Nanomedicine, Volume 14(), 5397–5413. doi:10.2147/IJN.S209662

(48). Tahari, Nadia; de Hoyos-Martinez, Pedro L.; Abderrabba, Manef; Ayadi, Sameh; Labidi, Jalel (2020). Lignin - montmorillonite hydrogels as toluene adsorbent. Colloids and Surfaces

A: Physicochemical and Engineering Aspects, (), 125108–. doi:10.1016/j.colsurfa.2020.125108

Table of Contents

Polysaccharide - Modified MMT/ Modified MMT/ Polysaccharide – MNP, Lignin - Modified MMT Nanocomposites Verses Polyethyleneimineimine- Modified MMT-: A Comparative Analysis of Sustained Pesticide Delivery

TOC

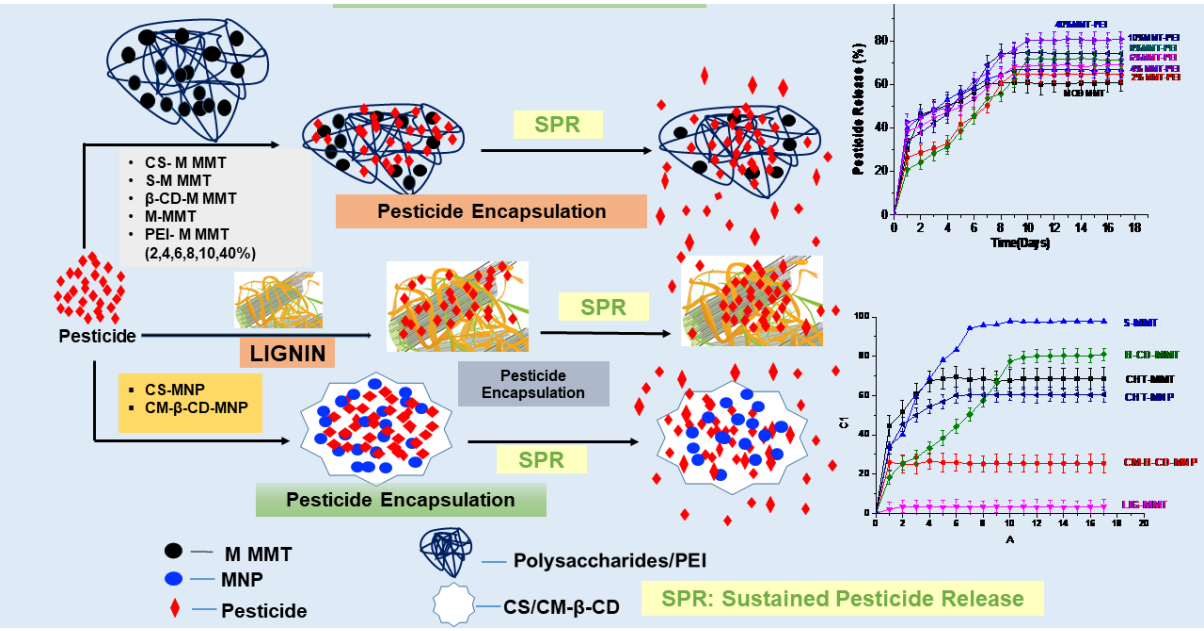

Highlights:

- At the nanoscale, the characteristics of a material can alter dramatically. With only a reduction in size and no change to the substance itself, materials can display new qualities.
- Polysaccharide-Modified MMT/ Modified MMT/ Polysaccharide – MNP, Lignin-Modified MMT Nanocomposites vs. Polyethyleneimineimine-Modified MMT have been compared for a Sustained Pesticide Delivery in this manuscript.
- We anticipate that this description will aid researchers in selecting the best technique for developing pesticides and improving pesticide delivery.